https://doi.org/10.5194/wes-2023-162
Preprint. Discussion started: 11 January 2024

eawe european academy of wind energy
Open Access WIND ENERGY SCIENCE DISCUSSIONS

Analysis of Turbine Yaw Misalignment Estimated by LIDAR Assuming Homogeneous Flow

Zhaoyu Zhang[1], Feng Guo[2], David Schlipf[2], Paolo Schito[1], and Alberto Zasso[1]

[1]Department of Mechanical Engineering, Politecnico di Milano, 20156 Milano, Italy
[2]Wind Energy Technology Institute, Flensburg University of Applied Sciences, 24943 Flensburg, Germany

Correspondence: Zhaoyu Zhang (zhaoyu.zhang@polimi.it)

Abstract. The 2D homogeneous flow assumption derived wind field reconstruction method is widely employed in the Doppler LIDAR. This paper aims to analyse the uncertainty in wind direction estimation and to improve the estimation accuracy. First, to quantify the uncertainty, a static model is proposed to describe the relationship between horizontal wind shear and yaw misalignment in LIDAR measurement. Subsequently, an analytic model of temporal-averaged misalignment uncertainty is built by using the Kaimal turbulence spectral model. This analytic model reveals that the standard deviation of yaw misalignment reaches approximately $\pm 14°$ and $\pm 12°$ for IEC turbulence class 'A' and 'B', respectively, regarding a temporal average over 60s. Obviously, these findings demonstrate that this LIDAR estimation method is insufficient to supervise the turbine yaw control system in terms of both accuracy and timeliness. Then, the temporal-averaged uncertainties obtained from the proposed analytic model are compared with simulations in various complexity, i.e. Kaimal, Mann spectral models, and Computational Fluid Dynamics, respectively. The rotor-average wind is set as the reference for measurement. Compared to an ideal sonic measurement, the LIDAR presents a worse estimation of rotor-effective wind direction estimation. These results show that increasing the fidelity of turbulence models does not alleviate the measurement uncertainty issue. Lastly, in an attempt to address the uncertainty issue, this study investigates the effects of adjusting the scanning pattern. The optimised parameters include measurement distance and horizontal half-open angle in a 2-beam LIDAR case and the additional vertical half-open angle in a 4-beam LIDAR case. However, even with the optimal scanning pattern, u and v wind components estimation could not acquire the same accuracy on the ideal sonic measurement simultaneously. Thereby, LIDAR can not guarantee wind speed and direction estimation quality simultaneously. In conclusion, this study highlights the yaw misalignment uncertainty in the LIDAR wind field reconstruction method based on 2D homogeneous flow assumption. The observed error levels remain consistent across varying fidelity turbulence models and scanning pattern adjustments. To address this challenge, future research should apply more advanced wind flow models to explore more accurate wind field reconstruction methods.

1 Introduction

The demand for wind energy is keeping increasing as an environment-friendly and renewable energy source. Wind turbines are equipped with a yaw control system and usually follow the changing wind direction. Wake and turbulence generated by upstream turbines in a wind farm cause 10% to 20% power loss (Barthelmie et al., 2009). Therefore, modern wind farm

https://doi.org/10.5194/wes-2023-162
Preprint. Discussion started: 11 January 2024

controller aim to reduce the wake interactions by misaligning the upwind turbines and by this redirecting the wind turbine wakes Fleming et al. (2017). Thus, for single turbines and wind farm control, the wind energy production highly depends on an accurate measurement of the wind direction.

There are several traditional measurement methods for the wind direction for wind turbines, such as nacelle-mounted cup anemometers or sonic anemometers. However, the measurement on the nacelle is becoming less and less representative of the increasing rotor sizes of modern wind turbines. The induction zone caused by turbine rotation as well as the flow distortion due to blades are also significant drawbacks for traditional measurement (Smith et al., 2006). In contrast, nacelle-based LIDAR (Light Detection and Ranging) systems measure in various points in front of the rotor and thus are expected to be more representative for large rotors and less impacted by the induction zone and rotating blades.

As a remote sensing technology, LIDAR measurement offers wind preview for control strategies designing that can be used to reduce turbine loads and optimize power production. Several improvements in control systems of wind farms benefited from reliable axial wind speed measurements from LIDAR. In many modern wind farms, the nacelle-based LIDAR has been implemented and verified in practical applications (Sathe et al., 2015). Assisted by the LIDAR measurement, Zhao et al. applied a wind turbine yaw strategy with adaptive yaw speed in a real wind farm. Implemented with the advanced yaw control system, Zhang and Yang investigated that the investment of LIDAR system can be covered by improving the power to be generated by the wind turbines within 2 years in a certain wind farm.

Wind field reconstruction by LIDAR currently relies on the 2D homogeneous flow assumption, in which the wind is assumed identical at the same height plane. LIDAR obtains the projection of wind speed along the Line Of Sight (LOS) of laser beams. Then, wind components, u and v, are estimated approximately back to real environment wind by applying the pseudo-inverse on LOS information (Raach et al., 2014).

However, a significant uncertainty in wind direction measurement of LIDAR is observed in several studies. The first reason is that the 2D homogeneous flow assumption does not consider the horizontal shear between two laser beams at the same height. Schlipf et al. compared the single probe record on turbine height with LIDAR simulation results applying the IEC Kaimal turbulence model. After applying a 1-minute average to measurement results, he found that the wind direction estimation of LIDAR does not show an advantage over a single probe because the horizontal shear caused misalignment.

Another reason is that the pseudo-inverse method could not fully revert speed projection to the real wind. In a spinner LIDAR experiment, Mikkelsen et al. found that the observed oscillation is caused by the increasing horizontal shear and a narrow cone angle. But this issue, so call ‘Cyclops’ problem, could be partially solved by tuning the open angle between two laser beams (Simley et al., 2011).

Some researchers have found the misalignment issue and attempted to solve it. To exclude the impact from different turbulence models, Dong et al. (2021) compared the LIDAR simulation results from Kaimal and Mann turbulence models respectively. However, the uncertainty issue did not be greatly improved. Towers and Jones (2016) replace the 2D homogeneous flow assumption with an advanced inflow model, such as Kalman filter-based dynamic inflow model. Moreover, a fast CFD (Computational Fluid Dynamics) solver-based inflow model is applied to reconstruct the wind field in real-time, which also reduces the LIDAR measurement uncertainty (Mikkelsen et al., 2016). However, these advanced inflow models are limited by the computational cost in a practical LIDAR application.

This study aims to analyse the reason for LIDAR measurement uncertainty and improve the wind turbine yaw misalignment issue. An analytic model is first proposed to describe the relationship between yaw misalignment and horizontal shear. Then, three turbulence models with different fidelity are applied and compared as the simulation environment for LIDAR measurement. Finally, an optimal LIDAR scan pattern is calculated after compared with the measurement quality of the sonic anemometer and rotor average wind. The analytic model and simulations of LIDAR measurement uncertainty have not been completely illustrated, although this topic has been explored in some previous research. This research, for the first time, focuses on the yaw misalignment analysis and improvement against the 2D homogeneous flow assumption-based wind field reconstruction.

This paper is organized as follows: In Section 2, relevant background information is provided such as LIDAR measurement models, the wind field reconstruction method, and turbulence models. Section 3 describes the relationship between LIDAR yaw misalignment and horizontal shear in a 2-beam LIDAR. Section 4 compares averaged yaw misalignment to avoid the effect of different turbulence models. In section 5, optimal scanning patterns for 2-beam and 4-beam LIDAR are proposed to minimize the measurement uncertainty. Finally, the conclusion and outlook are illustrated in Section 6.

2 Background

This section introduces previously developed models and methods, which are used in this work.

2.1 LIDAR point measurement model

Using the optical Doppler effect, a LIDAR system extracts the line-of-sight (LOS) wind speed along the laser beams. A simple point measurement model assumes a measurement in a single point i:

$$V_{\mathrm{los},i} = x_{n,i}u_i + y_{n,i}v_i + z_{n,i}w_i, \tag{1}$$

where $x_{n,i}$, $y_{n,i}$, and $z_{n,i}$ are the components of the normalized vector of the laser beam (pointing to the LIDAR system) in Cartesian coordinate system. Further, u_i, v_i, and w_i are the wind components in the measurement point i. This measurement model is usually used in wind field reconstruction.

2.2 LIDAR volume measurement model

In contrast to the simple point measurement model, real LIDAR systems extract the line-of-sight wind speed within a probe volume rather than in a single point. This is caused by the averaging effect by providing a certain fraction of the back-scattered signal to Fast Fourier transform (FFT)-based frequency shift detection, as well as by the pulse length for pulsed LIDAR systems (Sathe and Mann, 2012; Cariou, 2013).

https://doi.org/10.5194/wes-2023-162
Preprint. Discussion started: 11 January 2024

WIND ENERGY SCIENCE DISCUSSIONS
Open Access

The LOS measurement including the volume is modelled by

$$V_{\mathrm{los},i} = \int_{-\infty}^{\infty} \left(x_{n,i}u_i(a) + y_{n,i}v_i(a) + z_{n,i}w_i(a)\right) f_{\mathrm{RW}}(a)\,\mathrm{d}a, \tag{2}$$

where a is the distance between the local measurement point and focus point along the laser beam. Further, f_{RW} is the range weighting function along the variable a.

In this paper, we focus on pulsed LIDAR systems with a Full Width at Half Maximum (FWHM) of $W = 30m$. The weighting function is discretized in three points with the distances $[-\frac{1}{2}W, 0, \frac{1}{2}W]$ and the corresponding weight parameters of $[0.25, 0.5, 0.25]$.

2.3 2D homogeneous flow model

In current industrial applications, the 2 dimensions homogeneous flow model is usually applied to estimate yaw misalignment using LIDAR measurements (Lundquist et al., 2015). This model is widely applied in flat terrain and assumes that the longitudinal wind component u_i and lateral wind component v_i are the same for all points i within each horizontal plane, and the vertical wind components w_i are zero, i.e.

$$\begin{aligned} u_1 &= u_2 = \cdots = u_n = u \\ v_1 &= v_2 = \cdots = v_n = v \\ w_1 &= w_2 = \cdots = w_n = 0. \end{aligned} \tag{3}$$

2.4 Quasi-Static wind field reconstruction

Wind field reconstruction is the process of extracting information about the wind field from LIDAR measurements. It combines LIDAR and wind flow models. For the case of a horizontally nacelle-based LIDAR with 2 beams, the 2D homogeneous flow model from Equation (3) is combined with the simple LIDAR point measurement model from Equation 1.

$$\underbrace{\begin{bmatrix} V_{\mathrm{los},1} \\ V_{\mathrm{los},2} \end{bmatrix}}_{m} = \underbrace{\begin{bmatrix} x_{n,1} & y_{n,1} \\ x_{n,2} & y_{n,2} \end{bmatrix}}_{A} \underbrace{\begin{bmatrix} u \\ v \end{bmatrix}}_{s}. \tag{4}$$

The components of the normalized vector of the laser beam can be calculated by

$$\begin{aligned} x_{n,1} &= x_{n,2} = \cos(\theta_H) \\ y_{n,1} &= -y_{n,2} = -\sin(\theta_H) \\ z_{n,1} &= z_{n,2} = 0 \end{aligned} \tag{5}$$

θ_H is the horizontal half-open angle (HOA) between two beams and the vertical beam components are zero, because the LIDAR is scanning horizontally.

https://doi.org/10.5194/wes-2023-162
Preprint. Discussion started: 11 January 2024

From Equation 4, the longitudinal wind component u and the lateral wind component v can be reconstructed by a matrix inversion of matrix A. Consider horizontal shears, $\delta_\mathrm{H}\left(\mathrm{m}\cdot\mathrm{s}^{-1}\cdot\mathrm{m}^{-1}\right)$, is linear along the horizontal direction between two same-height beams. The resulting estimated longitudinal wind speed component is

$$\begin{aligned}\hat{u} &= \frac{x_{n1}y_{n2}}{x_{n1}y_{n2}-x_{n2}y_{n1}}(\bar{u}+\delta_\mathrm{H}d) - \frac{x_{n2}y_{n1}}{x_{n1}y_{n2}-x_{n2}y_{n1}}(\bar{u}-\delta_\mathrm{H}d)\\ &= \bar{u} - \frac{x_{n1}y_{n2}+x_{n2}y_{n1}}{x_{n1}y_{n2}-x_{n2}y_{n1}}\delta_\mathrm{H}d\\ &= \bar{u}+\Theta_1\delta_\mathrm{H}d\end{aligned} \tag{6}$$

and the estimated lateral wind speed component is

$$\begin{aligned}\hat{v} &= \frac{-x_{n1}x_{n2}}{x_{n1}y_{n2}-x_{n2}y_{n1}}(\bar{u}+\delta_\mathrm{H}d) + \frac{x_{n1}x_{n2}}{x_{n1}y_{n2}-x_{n2}y_{n1}}(\bar{u}-\delta_\mathrm{H}d)\\ &= -\frac{-2x_{n1}x_{n2}}{x_{n1}y_{n2}-x_{n2}y_{n1}}\delta_\mathrm{H}d\\ &= \Theta_2\delta_\mathrm{H}d\end{aligned} \tag{7}$$

where Θ_1 and Θ_2 are constant derived on the scanning pattern of LIDAR

$$\begin{aligned}\Theta_1 &= -\frac{x_{n1}y_{n2}+x_{n2}y_{n1}}{x_{n1}y_{n2}-x_{n2}y_{n1}}\\ \Theta_2 &= -\frac{-2x_{n1}x_{n2}}{x_{n1}y_{n2}-x_{n2}y_{n1}}\end{aligned} \tag{8}$$

It reveals that the estimation of speed components only depends on the horizontal wind shear δ_H and the scanning pattern of LIDAR. The method is named 'quasi-static' because no dynamic model is used, but it is assumed that the wind is the same in the two points.

2.5 Kaimal spectrum and exponential coherence model

As one of the International Electrotechnical Commission (IEC) Standard recommended turbulence models (Commission et al., 2005), the Kaimal spectrum and exponential coherence model shows concise theory and low computational cost in wind energy system design areas (Kaimal et al., 1972). The non-dimensional power spectral densities (PSDs) for three wind components are shown as

$$\frac{fS_k(f)}{\sigma_k^2} = \frac{4fL_k/V_\mathrm{hub}}{(1+6fL_k/V_\mathrm{hub})^{5/3}}, \tag{9}$$

where f is the frequency, k represents the wind component direction (1 for longitudinal u, 2 for lateral v, and 3 for vertical w). Further, σ and L are the standard deviation and integral scale parameter, respectively. In this paper, the wind speed at turbine hub height V_hub is set to 10m/s.

2.6 Mann uniform shear turbulence model

Another turbulence model recommended by the IEC Standard is the Mann uniform shear turbulence model (Mann, 1994, 1998), which is used for comparison with the Kaimal model in this paper.

https://doi.org/10.5194/wes-2023-162
Preprint. Discussion started: 11 January 2024

The Mann uniform shear turbulence model is a spectral tensor model based on von Kármán's model and linearized Navier-Stokes (N-S) equations (Von Karman, 1948). It is an integration of eddy lifetimes and rapid distortion theory by assuming the incompressible flow. The 3D velocity wind components are defined as the summation of average wind speed and 3D fluctuations caused by turbulence. The spectral tensor is shown by the following equation:

$$\Phi_{i,j}(k) = \frac{1}{(2\pi)^3} \int R_{i,j}(r) e^{-ik\cdot r} \mathrm{d}r, \tag{10}$$

where R is the covariance tensor and r is separation vector, k is non-dimensional spatial wave-parameter.

2.7 Large eddy simulation

Large Eddy Simulation (LES) is a high-fidelity mathematical model as a Computational Fluid Dynamics (CFD) approach. The dynamic turbulence simulation is built by solving Navier–Stokes (NS) equations numerically (Piomelli, 1999; Zhang et al., 2022). An LES-based low-pass filter is applied to reduce the computational cost by eliminating small-scale items. This method makes it possible to be widely used in many areas with a reasonable computational cost.

In this paper, the LIDAR estimated misalignment model is verified in LES simulation and compared with results from lower fidelity models.

3 Yaw misalignment estimation models

This section describes the models developed in this work to estimate the yaw misalignment of wind turbines using the homogenous flow model from Section 2.3.

3.1 Static yaw misalignment model due to horizontal shear

In a realistic environment, the assumptions of the 2D homogeneous flow model from Equation (3) are not perfectly fulfilled. The difference in the longitudinal u wind speeds components horizontally, here characterized as horizontal shear, is mainly depending on the turbulence characteristics. As a result, the homogeneous assumption leads to errors in the wind field reconstruction. In this subsection, a measurement uncertainty model is built to determine the impact of the horizontal shear on wind speed and direction estimation of a 2-beam LIDAR system.

Here we assume that the flow deviates from the of the 2D homogeneous flow model from Equation (3) in the following form:

$$\begin{aligned} u_1 &= \bar{u} + \delta_{\mathrm{H}} d \\ u_2 &= \bar{u} - \delta_{\mathrm{H}} d \\ v_1 &= v_2 = 0 \\ w_1 &= w_2 = 0. \end{aligned} \tag{11}$$

where $\bar{u}$ is the mean longitudinal wind speed and $d = \tan(\theta_H)L$ is the horizontal distance from the horizontal center point to one of the measurement focus points, where L is the LIDAR measurement distance. We further consider δ_{H}, is to be the linear horizontal shear. The lateral and vertical wind speed components are considered to be zero for simplicity.

With the LIDAR point measurement model from Equation (1), we obtain following line-of-sight wind speeds for the two-beam LIDAR system:

$$\begin{aligned} V_{\mathrm{los},1} &= x_{n,i}(\bar{u} + \delta_{\mathrm{H}} d) \\ V_{\mathrm{los},2} &= x_{n,i}(\bar{u} + \delta_{\mathrm{H}} d) \end{aligned} \tag{12}$$

Then, substituting the line-of-sight wind speeds in Equation (4) with the ones from Equation (12) and applying a matrix inversion, the estimated longitudinal wind speed component is

$$\begin{aligned} \hat{u} &= \frac{x_{n,1}y_{n,2}}{x_{n,1}y_{n,2} - x_{n,2}y_{n,1}}(\bar{u} + \delta_{\mathrm{H}} d) \\ &\quad - \frac{x_{n,2}y_{n,1}}{x_{n,1}y_{n,2} - x_{n,2}y_{n,1}}(\bar{u} - \delta_{\mathrm{H}} d) \\ &= \bar{u} \end{aligned} \tag{13}$$

and the estimated lateral wind speed component is

$$\begin{aligned} \hat{v} &= \frac{-x_{n,1}x_{n,2}}{x_{n,1}y_{n,2} - x_{n,2}y_{n,1}}(\bar{u} + \delta_{\mathrm{H}} d) \\ &\quad + \frac{x_{n,1}x_{n,2}}{x_{n,1}y_{n,2} - x_{n,2}y_{n,1}}(\bar{u} - \delta_{\mathrm{H}} d) \\ &= 2\delta_{\mathrm{H}} d \end{aligned} \tag{14}$$

The estimated wind speed and yaw misalignment considering horizontal shear are shown as

$$V = \sqrt{\hat{u}^2 + \hat{v}^2} \quad , \quad \alpha_{\mathrm{H}} = \tan\left(\frac{\hat{u}}{\hat{v}}\right). \tag{15}$$

Compared with the wind assumed wind conditions at the centre point, homogeneous assumption based estimation errors are

$$\begin{aligned} \varepsilon_u &= \hat{u} - \bar{u} = 0 \\ \varepsilon_v &= \hat{v} - \bar{v} = 2\delta_{\mathrm{H}} d - \bar{v} \end{aligned} \tag{16}$$

Component errors indicate that only the v component is affected by the horizontal shear in a linear manner, shown in Figure 1. Therefore, the wind speed estimation V is slightly influenced by the horizontal shear, because the $\hat{u}$ component plays a majority role in Equations 15, i.e. $\hat{u} >> \hat{v}$. In contrast, wind direction estimation α_H earns a significant misalignment. Figure 2 shows that the misalignment up to $10°$ as horizontal shear is 0.02 $\mathrm{m \cdot s^{-1} \cdot m^{-1}}$. The static misalignment model is shown below,

$$\begin{aligned} \triangle\alpha_H &= \mathrm{atan}\left(\frac{\bar{u}_1}{\bar{v}_1}\right) - \mathrm{atan}\left(\frac{\bar{u}_1 + \varepsilon_u}{\bar{v}_1 + \varepsilon_v}\right) \\ &= 0.5\pi - \mathrm{atan}\left(\frac{\bar{u}_1}{2\delta_H d}\right) \end{aligned} \tag{17}$$

https://doi.org/10.5194/wes-2023-162
Preprint. Discussion started: 11 January 2024

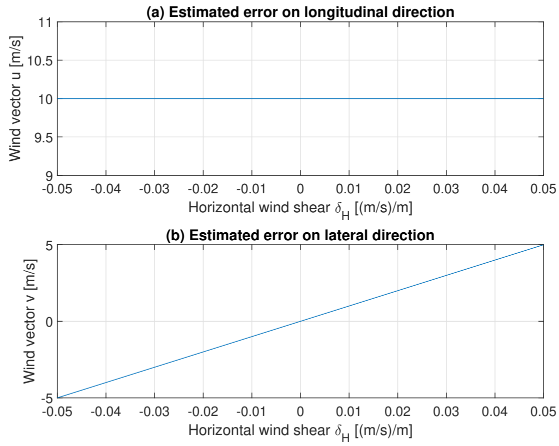

Figure 1. Estimated wind components errors caused by horizontal shear

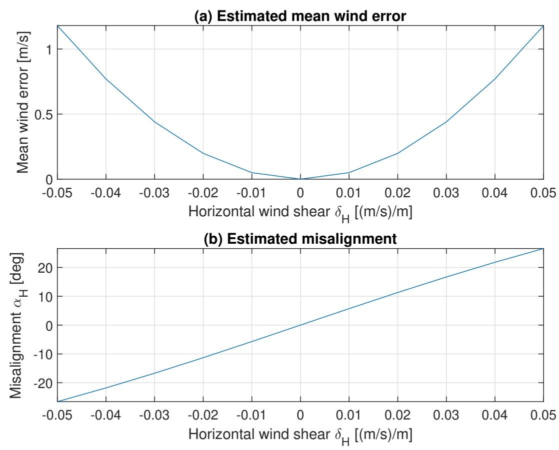

Figure 2. Estimated wind speed and direction errors caused by horizontal shear

This low-accuracy situation has not attracted enough attention in the current measurement and yaw control area. In this paper, the horizontal shear caused wind direction estimation error is analysed and improved.

3.2 Spectral model of horizontal shear

The horizontal shear between two LIDAR beams along the lateral direction is $e(t) = u_1(t) - u_2(t)$. The auto-spectral density of wind components is identical in a certain turbulence model (Schlipf, 2016), i.e. $S_{u1} = S_{u2} = S_u$. Then, the magnitude-squared coherence of u components between two points is defined as

$$C_{u1,2}^2 = \frac{\mathcal{R}^2(S_{u1,2})}{S_{u1}S_{u2}} = \frac{\mathcal{R}^2(S_{u1,2})}{S_u^2} \tag{18}$$

https://doi.org/10.5194/wes-2023-162
Preprint. Discussion started: 11 January 2024

where function $\mathcal{R}$ calculates the magnitude of the spectral density, $S_{u1,2}$ is cross-spectral density of u component between two points.

The auto-spectral density of horizontal shear, S_e, is derived by the product of Fourier Transform $\mathcal{F}(e)$ and its complex conjugate $\mathcal{F}^*(e)$ (Chen et al., 2022). Then, substituting the equation 20,

$$\begin{aligned} S_e &= \mathcal{F}(e)\mathcal{F}^*(e) \\ &= (\mathcal{F}(u_1) - \mathcal{F}(u_2))(\mathcal{F}^*(u_1) - \mathcal{F}^*(u_2)) \\ &= S_{u1} + S_{u2} - 2\mathcal{R}(S_{u1,2}) \\ &= 2S_u(1 - C_{u1,2}) \end{aligned} \tag{19}$$

In this paper, the horizontal wind speed uncertainty U_e is defined as twice standard deviation within 95.45% confidence interval. The standard deviation is square root of variance which is the integral of the auto-spectrum S_e, i.e.

$$U_e = 2\sigma(e) = 2\sqrt{\int_{-\infty}^{\infty} S_e \mathrm{d}f} \tag{20}$$

Then substituting Equation 17 and replacing the horizontal wind speed difference ε_u with averaged wind speed uncertainty U_e in Equation 20, the average misalignment estimation can also be evaluated.

3.3 Temporal-averaged misalignment uncertainty model

In addition to the LIDAR average misalignment derivation, different averaging time based statistical misalignment has significant guidance on trend analysis and error elimination. In this section, the approximated moving average of e during the time window T is calculated by a convolution ($*$) (Schlipf et al., 2020), shown as

$$\overline{e}(t) = e(t) * \mathrm{rect}\left(\frac{t - T/2}{T}\right) \tag{21}$$

where $\mathrm{rect}()$ is time depended rectangular function

$$\mathrm{rect}(t) = \begin{cases} 1, & \left|t\right| \leq 0.5 \\ 0, & \left|t\right| > 0.5 \end{cases} \tag{22}$$

From Equation 21, the auto-spectrum of averaged horizontal shear, $S_{\overline{e}}$, is calculated by product of Fourier Transform $\mathcal{F}(\overline{e})$ and complex conjugate $\mathcal{F}^*(\overline{e})$. Moreover, the convolution could be derived as the product of the Fourier transform as a linear operator. The auto-spectrum $S_{\overline{e}}$ is rewrote as following considering the difference averaging time T,

$$\begin{aligned} S_{\overline{e}} &= \mathcal{F}(\overline{e})\mathcal{F}^*(\overline{e}) \\ &= \mathcal{F}(e)\mathcal{F}^*(e)\,\mathrm{sinc}^2(fT) \\ &= 2S_u(1 - C_{u1,2})\,\mathrm{sinc}^2(fT) \end{aligned} \tag{23}$$

https://doi.org/10.5194/wes-2023-162
Preprint. Discussion started: 11 January 2024

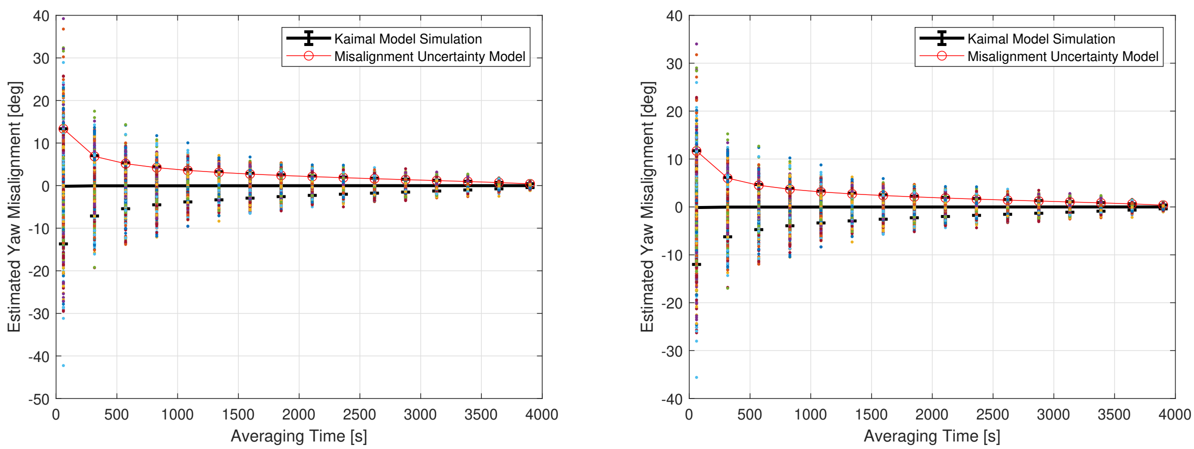

Figure 3. Kaimal model based temporal-averaged misalignment uncertainty with IEC standard turbulence class ’A’ (left) and ’B’ (right)

where function sinc is the normalized cardinal sine function. S_u and $C_{u1,2}$ are obtained by a certain turbulence model. Then substituting Equation 17 and 20, the averaged horizontal shear and its misalignment estimation can also be calculated in sequence.

In this paper, the Kaimal turbulence based Misalignment Uncertainty Model is defined as a reference to compare different turbulence environments and LIDAR scanning patterns, since the low computational cost Kaimal turbulence model (in section **??**) and a clear calculation processing (in section 3.2). According to the IEC standard, turbulence conditions are divided into several classes based on wind speed and turbulence intensity (TI), such as class ’A’ for 0.18 TI and class ’B’ for 0.16 TI (Dimitrov et al., 2015).

Derived using auto spectrum S_u and coherence $C_{u1,2}$ from the Kaimal model, the Misalignment Uncertainty Model is indicated by the red line in Figure 3. Additionally, the Misalignment Uncertainty Model is validated through simulations. The Kaimal turbulence is generated randomly by different computer random seeds, in which the wind difference between two beams is recorded. The figure also demonstrates the misalignment within various temporal average windows. Simulation results are represented by colourful points, while the standard deviation is shown by black error bars.

The results reveal that during the 60s time window, the misalignment reaches a standard deviation of around $\pm 14°$ and $\pm 12°$ regarding turbulence class ’A’ and ’B’, respectively. Even when the temporal average window increased to 600s, the standard deviation of misalignment is still around $\pm 5°$ and $\pm 6°$.

In conclusion, the Misalignment Uncertainty Model model demonstrates that the homogeneous flow assumption derived wind field reconstruction of LIDAR can not fulfil the requirement for yaw control, because the yaw misalignment is too large to be dismissed by a moving average filter. This analysis presents a significant challenge in the field of LIDAR measurement and turbine control. To identify the possible reasons and avoid the effect of specific setups and environments, different turbulence models and LIDAR scanning patterns are evaluated in the next two sections.

https://doi.org/10.5194/wes-2023-162
Preprint. Discussion started: 11 January 2024

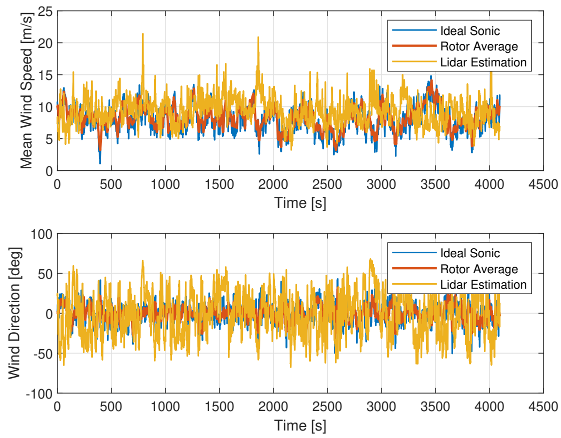

Figure 4. LIDAR estimation comparison with rotor average and ideal sonic in Mann model with 0.35 turbulence intensity

4 Turbulence model comparison for 2-beam LIDAR

To determine and quantify the effects of horizontal shear on wind direction estimation, there are several approaches for building a turbulence environment. Two of them, Kaimal model and Mann model, are employed by International Electrotechnical Commission (IEC) standard, in which the wind energy generation system is designed and normalized. Moreover, the Large Eddy Simulation (LES) is also widely used for high-fidelity turbulence simulation using a mathematical model in Computational Fluid Dynamics (CFD).

In this section, the Kaimal turbulence based Misalignment Uncertainty Model is compared with simulation results of Mann model and LES. The initial LIDAR scanning pattern sets measurement distance L as 100m, horizontal half open angle θ_H as $15°$.

4.1 Mann model derived yaw misalignment

A 4-Dimensions Mann model derived turbulence generator is developed by fengguoFUAS (2022), which is an open-source tool running on MATLAB. The turbulence parameters and wind field scale, etc are fully manipulated in this tool. To enable a direct comparison of results, the simulation time and turbulence intensity are set to match those used in the simulation of Kaimal model.

In this simulation, a virtual LIDAR on the nacelle reconstructs the wind field by reading interpolated wind information. A simulation probe is located at the turbine height to emulate an ideal sonic anemometer which has no measurement errors or system errors. As a reference, the wind speed and direction on the rotor plane are averaged following mesh resolution. Comparison results of wind speed and direction estimation are shown in Figure 4.

Results illustrate that the mean wind speed estimation of LIDAR mostly follows the temporal-averaged wind on the rotor plane, even though it is not as accurate as the ideal sonic anemometer. Considering the significant measurement errors of sonic

https://doi.org/10.5194/wes-2023-162
Preprint. Discussion started: 11 January 2024

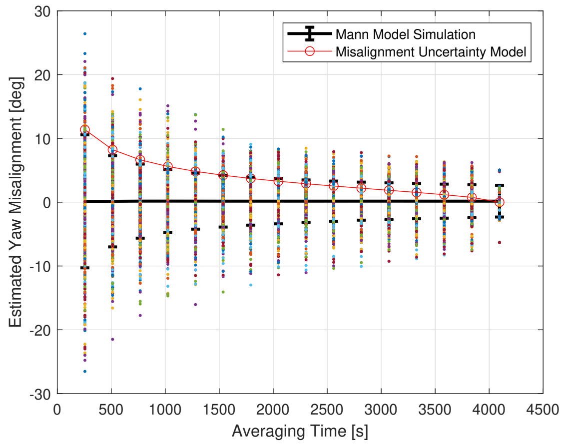

Figure 5. Mann model based temporal-averaged misalignment uncertainty with 0.35 turbulence intensity

anemometers and the effects of the induction zone during the real operation of the turbine, LIDAR earns much more advantages on wind speed estimation than sonic anemometers.

255 However, there is a large error in the wind direction estimation of LIDAR, which is difficult to guide the turbine yaw control. In the real wind direction measurement, the data is typically filtered by a low-pass filter, such as the moving average filter. The pass frequency of the filter is controlled by the temporal-averaged window, which is designed regarding LIDAR measurement distance and wind speed. Based on simulation results in Figure 4 and misalignment estimation in Equation 17, the measurement misalignment within different temporal-averaged windows are shown in Figure 5.

260 To eliminate the effect of random turbulence on misalignment statistics, 20 turbulence simulations are recorded and generated using the different computer random seeds. As a result, the mean misalignment is approximately 0. The standard deviation with the large averaging time is larger than the result of a single simulation.

Excluding the impact of multi-simulations statistics, the Kaimal model derived Misalignment Uncertainty Model and temporal-averaged simulation results of Mann model are consistently consistent under the various turbulence intensity, shown in Figure 265 6.

4.2 LES derived yaw misalignment

Limited by the computational cost requirement, the LES turbulence environment was reconstructed from an open-science data set provided by the Technical University of Denmark (Andersen, 2020). The 3-dimensions wind components in the simulation wind field were extracted using MATLAB. After simple interpolation on the simulation mesh, the full field wind information 270 was obtained (Liew et al., 2020).

In contrast to simulations based on Kaimal model and Mann model, the turbulence intensity is 0.028 in LES data set. The comparison between LIDAR estimation, ideal sonic and rotor average is shown in Figure 7. The estimation of both wind speed

https://doi.org/10.5194/wes-2023-162
Preprint. Discussion started: 11 January 2024

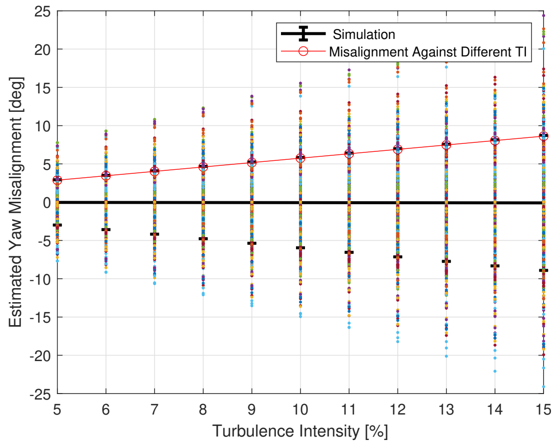

Figure 6. Misalignment against various turbulence intensity with 10m/s wind speed

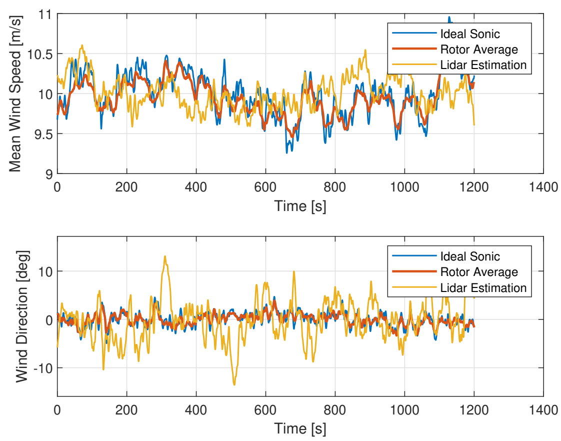

Figure 7. LIDAR estimation comparison with rotor average and ideal sonic in LES model with 0.028 turbulence intensity

and direction have much less error because of the smaller horizontal shear in the LES data set. However, the uncertainty in wind direction estimation is still significant.

The Kaimal based Misalignment Uncertainty Model is rebuilt following the same turbulence intensity of LES simulation. The LES-based misalignment with different temporal-averaged windows is shown in Figure 8.

As the LES data set consists of only one simulation, the results do not reflect the exact statistics. For instance, the mean of misalignment is not 0. Nonetheless, it is evident that the trend of LES-based misalignment approximately follows the Kaimal model-based Misalignment Uncertainty Model.

https://doi.org/10.5194/wes-2023-162
Preprint. Discussion started: 11 January 2024

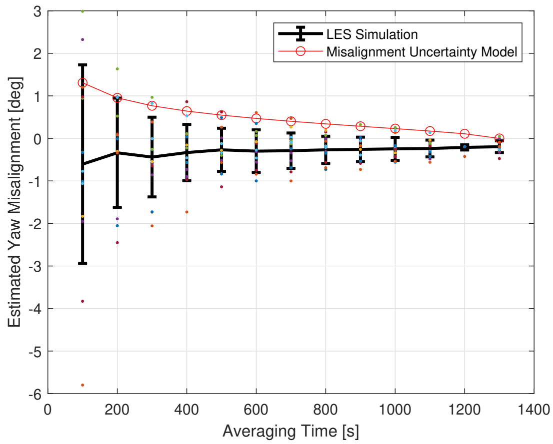

Figure 8. LES-based temporal-averaged misalignment uncertainty with 0.028 turbulence intensity

In conclusion, the yaw misalignment of LIDAR estimation produces similar results with different turbulence models. Hence, it can be inferred that the misalignment is mainly contributed by the LIDAR scanning pattern or wind reconstruction method rather than turbulence simulations.

5 Analysis for more complex LIDAR scanning pattern

This section aims to analyze the significant yaw misalignment and explore the reasons behind it by tuning the LIDAR scanning pattern. There are three factors that affect the quality of wind direction measurement with respect to the horizontal shear, i.e. measurement distance, open angle between beams and number of beams.

5.1 Quality evaluation of LIDAR and sonic

In this paper, the temporal-averaged wind on the rotor plane is calculated as the reference of inflow wind. From Equation 18, the quality of LIDAR measurement is evaluated using the coherence between LIDAR-estimated wind and rotor-averaged wind (C^2_{RL}) (Guo et al., 2022). Similarly, the quality of ideal sonic anemometer measurement is defined by the coherence between its measurement result and rotor-averaged wind (C^2_{Rs}), i.e.

$$C^2_{RL} = \frac{\mathcal{R}^2(S_{RL})^2}{S_{RR}S_{LL}} \quad , \quad C^2_{RS} = \frac{\mathcal{R}^2(S_{RS})^2}{S_{RR}S_{SS}} \tag{24}$$

Furthermore, to simplify the calculation, the quality of LIDAR measurement is rewritten in a transfer function (Simley and Pao, 2013),

$$T_{RL} = \frac{\mathcal{R}(S_{RL})}{S_{LL}} \quad , \quad T_{RS} = \frac{\mathcal{R}(S_{RS})}{S_{SS}} \tag{25}$$

https://doi.org/10.5194/wes-2023-162
Preprint. Discussion started: 11 January 2024

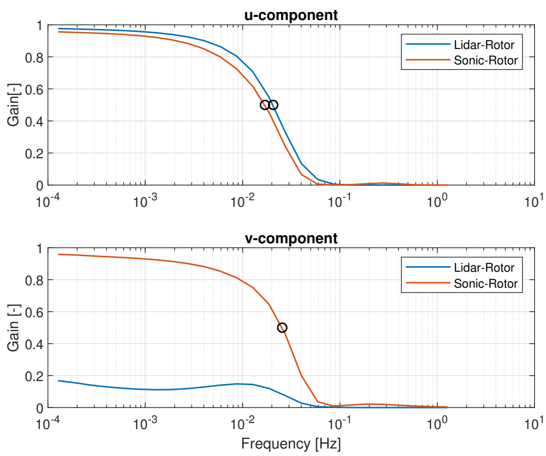

Figure 9. Transfer function comparison between LIDAR and Sonic with original scanning pattern of 2-beam LIDAR

In an ideal measurement process, gains of T_{RL} and T_{RS} should be 1 for all frequencies. However, in the simulation or practical measurement, the results are affected by measurement errors and wind uncertainty. Similar to a low-pass filter, the transfer functions of LIDAR and Sonic are considered of good quality only if they have high gains in a wide low-frequency range.

5.2 LIDAR scanning pattern optimization

The current LIDAR scanning pattern has a measurement distance of 100m and a horizontal half-open angle (HOA) of 15°. only the u component has an effective gain on low-frequency, shown in Figure 9. The small gain during low frequency on the v component causes dominant misalignment uncertainty.

Based on Equation 18, a Measurement Coherence Bandwidth (MCB) is defined as the frequency when the coherence (gain) drops to 0.5 (Guo et al., 2023). The MCB is usually used as a criterion to evaluate the measurement quality of LIDAR. Black circles illustrate points that reach 0.5 coherence in Figure 9.

To ensure that both wind speed and direction estimation of LIDAR are more robust than the ideal sonic anemometer, the transfer function between rotor-averaged wind and LIDAR estimation (shown by LIDAR-Rotor) should have a larger gain on low-frequency than the transfer function between rotor-averaged wind and ideal anemometer record (shown by Sonic-Rotor), i.e. a larger MCB.

5.2.1 2-Beam LIDAR verification

The horizontal half-open angle (HOA) between two beams and measurement distance are key parameters of yaw misalignment estimation for a 2-beam LIDAR. In this section, brute force optimization is applied to find an optimal LIDAR scanning pattern, in which both u and v components of LIDAR estimation have better low-pass performance than the ideal sonic anemometer.

https://doi.org/10.5194/wes-2023-162
Preprint. Discussion started: 11 January 2024

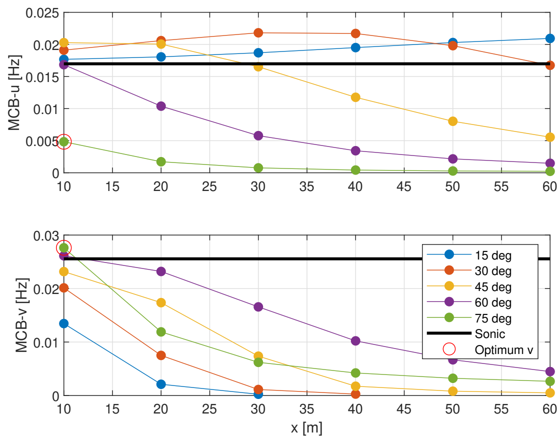

Figure 10. Scanning patterns comparison of 2-beam LIDAR

To simplify the comparison of transfer functions and signal qualities, the MCB is set as a threshold to determine the effective low-pass frequency. Hence, the transfer function of an accurately estimated signal should have a larger frequency when the gain reaches 0.5, i.e. the rotor-averaged wind is estimated effectively in a wider frequency range.

Then, frequencies at 0.5 gain, MCB, with different scanning patterns are extracted into Figure 10. Colourful lines represent different horizontal half-open angles between two LIDAR beams, while the x-axial shows different measurement distances. As a comparison reference, the black line represents the effective frequency of the Sonic-Rotor transfer function.

From Figure 10, the LIDAR estimation quality of v component declines as the measurement distance increases or the half-open angle drops until 60°. The optimal v component estimation happens with 10m measurement distance and 75° half-open angle, full of frequency analysis is shown in Figure 11. At this condition, the wind direction is well estimated by LIDAR for an optimal v component performance. While the wind speed estimation should not as perfect as the ideal sonic because of the lower effective frequency of the u component.

Based on the analysis, it can be concluded that there is no scanning pattern that ensures both u and v components have larger effective frequencies than the ideal sonic anemometer. Even though the LIDAR estimation has fewer errors when the measurement distance is small, such as 10m. This scanning pattern will be not applied to industries since it loses the prediction characteristics of LIDAR.

5.2.2 4-Beam LIDAR verification

To design a 4-beam LIDAR scanning pattern, except for the measurement distance (x) and horizontal half-open angle (HOA), the vertical half-open angle (VOA) should be considered. Similar to the analysis of the 2-beam LIDAR, the comparison result of the 4-beam LIDAR is shown in Figure 12. The optimal effective frequency of the v component is recorded by 20m measurement distance, 60° HOA and 30° VOA. However, the LIDAR estimation quality of the u component is far from the ideal sonic.

https://doi.org/10.5194/wes-2023-162
Preprint. Discussion started: 11 January 2024

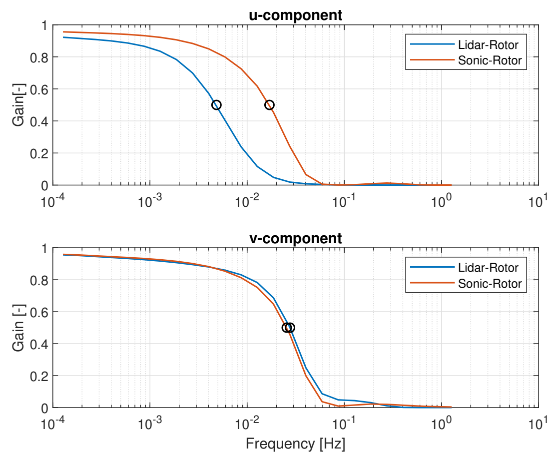

Figure 11. Transfer function of 2-beam LIDAR with optimal scanning pattern

The increasing measurement distance (x) takes the main factor for the decline in v component estimation quality. Similar to the trend observed in 2-beam LIDAR, the optimal HOA is around $50°$ $60°$, and optimal VOA is approximately $20°$ $30°$. However, both short measurement distance and large VOA result in the lack of remote sensing capability. Since local optimization only considers the performance of the v component, there is no practical solution for the LIDAR scanning pattern that ignores the performance of the u component.

In a global optimisation that considers both u and v components, two LIDAR scanning pattern solutions have larger frequencies at 0.5 gain (MCB) points than ideal sonic, shown in Figure 13. However, their v components demonstrate a sharp drop during the low-frequency range. The LIDAR estimation should have less low-frequency uncertainty than the ideal sonic, especially on wind direction estimation. Compared to Figure 11, the 4-beam LIDAR shows more potential for manipulation on yaw misalignment elimination than the 2-beam LIDAR, even though it fails in comparison to the ideal sonic.

6 Conclusion and outlook

In this study, the static yaw misalignment model is proposed to investigate the relationship between yaw misalignment and horizontal wind shear, which is built using a 2D homogeneous flow model based on 2-beam LIDAR estimation. This model indicates that the wind speed estimation does not affect by the horizontal shear, while the wind direction estimation shows a nonlinear change.

To evaluate the impact of turbulent wind environments on LIDAR estimation misalignment, we developed the Misalignment Uncertainty Model, which is derived from the horizontal wind shear determined by the Kaimal spectrum turbulence model. After averaging over different time windows, results show that the error reduces as the averaging time window size increases. However, misalignment is still significant which makes it challenging to supervise the yaw control of turbines from LIDAR measurement.

https://doi.org/10.5194/wes-2023-162
Preprint. Discussion started: 11 January 2024

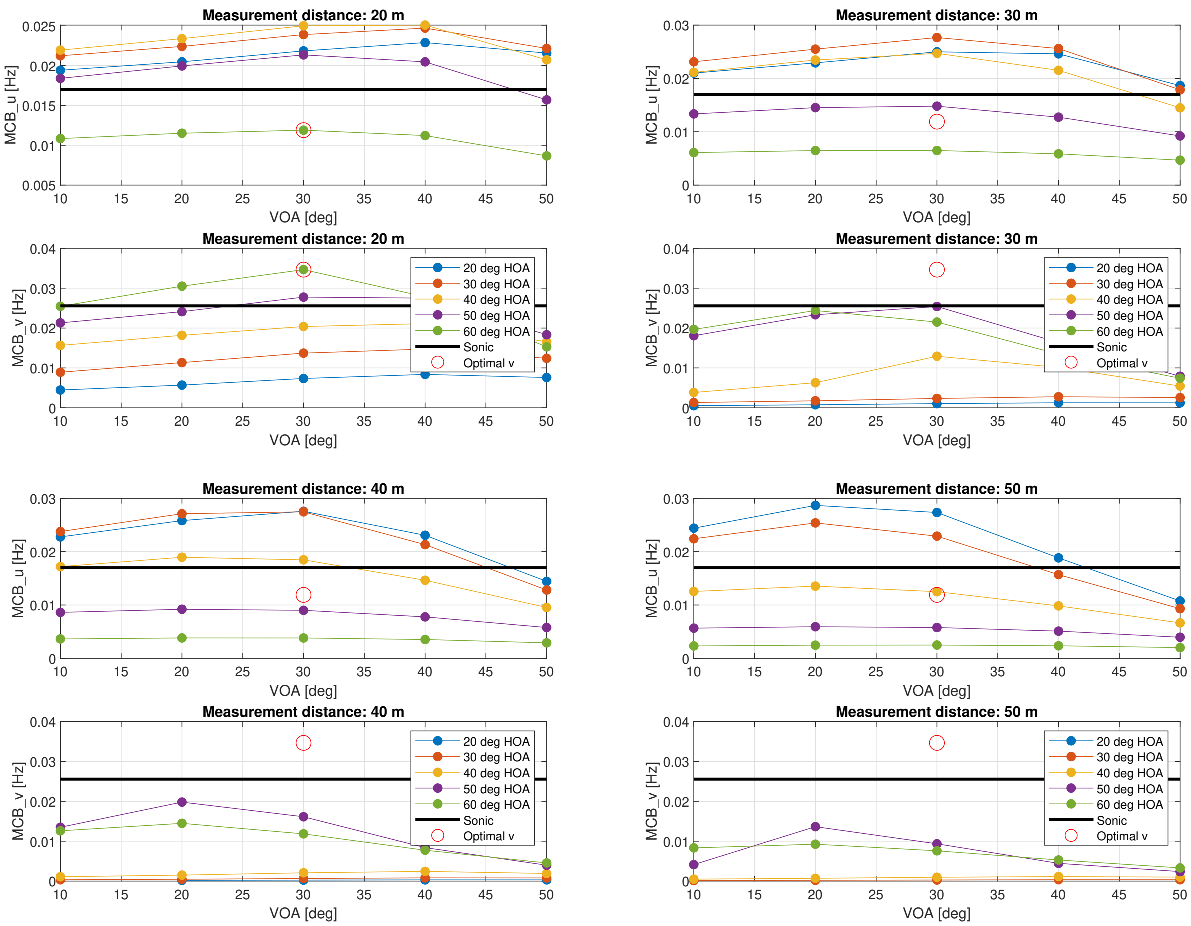

Figure 12. Scanning patterns comparison of 4-beam LIDAR

355 We verified the proposed analytic Misalignment Uncertainty Model through simulations using various turbulence models, including the Kaimal model, Mann model, and LES. The comparison results show consistency, indicating a similar trend in misalignment across turbulence models in different fidelity.

Furthermore, we applied coherence analysis between LIDAR estimation and rotor-averaged wind to mitigate estimation uncertainty, particularly in wind direction. We optimized the LIDAR scanning pattern parameters, including horizontal half
360 open-angle, measurement distance in a 2-beam LIDAR, and additional vertical half open-angle in a 4-beam LIDAR. The optimal solution of the 4-beam LIDAR scanning pattern improved estimation robustness compared to the 2-beam LIDAR. However, the estimated uncertainty of the LIDAR measurements remained larger than that of the ideal sonic anemometer, which challenges current LIDAR research expectations.

In conclusion, our study demonstrates that the 2D homogeneous flow assumption-based wind reconstruction does not achieve
365 superior accuracy in LIDAR measurements compared to ideal sonic anemometers in simulations, primarily due to the influ-

https://doi.org/10.5194/wes-2023-162
Preprint. Discussion started: 11 January 2024

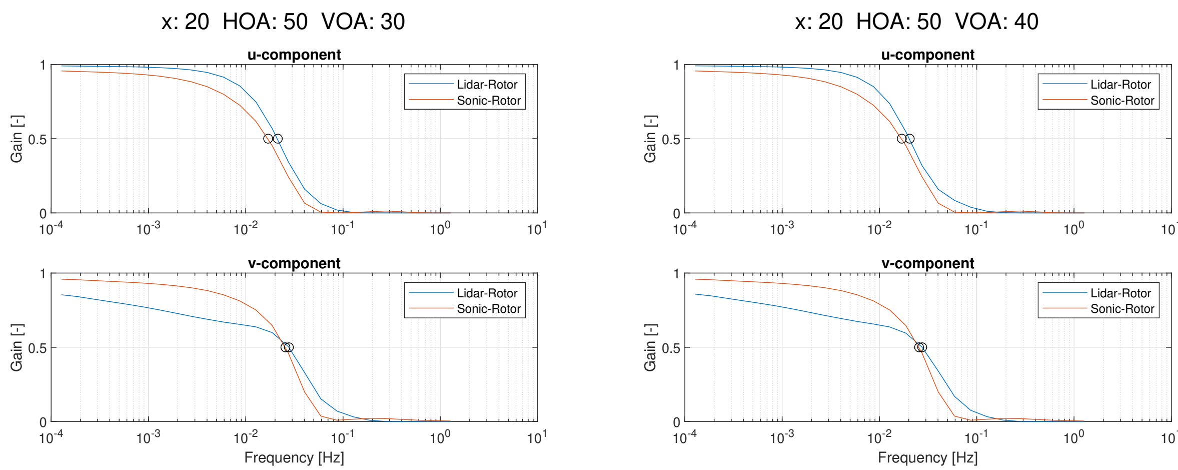

Figure 13. Transfer functions of 4-beam LIDAR with two optimal scanning patterns

ence of horizontal shear. Nonetheless, this paper successfully detects and analyzes significant yaw misalignment in LIDAR estimation, providing crucial insights for LIDAR simulation and turbine yaw control studies. Future research should focus on addressing the impact of horizontal shear on wind direction estimation by employing advanced dynamic wind flow models and realistic cup anemometer simulations.

Author contributions. ZZ performed simulations and drafted the manuscript. FG contributed to simulations and paper reviews. DS assisted in conceiving the overall concept, building the spectral model, and simulations. PS and AZ helped with the LES simulations and paper reviews.

Competing interests. The contact author has declared that none of the authors has any competing interests.

Acknowledgements. This project has received funding from the European Union's Horizon 2020 research and innovation program under the Marie Skłodowska-Curie grant agreement No.858358 (LIKE – Lidar Knowledge Europe).

https://doi.org/10.5194/wes-2023-162
Preprint. Discussion started: 11 January 2024

References

Andersen, S. J.: LES of wake flow behind 2.3MW wind turbine, https://doi.org/10.11583/DTU.12005421.v1, 2020.

Barthelmie, R. J., Hansen, K., Frandsen, S. T., Rathmann, O., Schepers, J., Schlez, W., Phillips, J., Rados, K., Zervos, A., Politis, E., et al.: Modelling and measuring flow and wind turbine wakes in large wind farms offshore, Wind Energy: An International Journal for Progress and Applications in Wind Power Conversion Technology, 12, 431–444, 2009.

Cariou, J.-P.: Pulsed lidars, Remote Sensing for Wind Energy, DTU Wind Energy-E-Report-0029 (EN), pp. 104–121, 2013.

Chen, Y., Guo, F., Schlipf, D., and Cheng, P. W.: Four-dimensional wind field generation for the aeroelastic simulation of wind turbines with lidars, Wind Energy Science, 7, 539–558, 2022.

Commission, I. E. et al.: Wind turbines-part 1: design requirements, IEC 61400-1 Ed. 3, 2005.

Dimitrov, N., Natarajan, A., and Kelly, M.: Model of wind shear conditional on turbulence and its impact on wind turbine loads, Wind Energy, 18, 1917–1931, https://doi.org/10.1002/we.1797, 2015.

Dong, L., Lio, W. H., and Simley, E.: On turbulence models and lidar measurements for wind turbine control, Wind Energy Science, 6, 1491–1500, https://doi.org/10.5194/wes-6-1491-2021, 2021.

fengguoFUAS: fengguoFUAS/4D-Mann-Turbulence-Generator: Initial release of the 4DMann Turbulence Generator, https://doi.org/10.5281/zenodo.6223785, 2022.

Fleming, P., Annoni, J., Shah, J. J., Wang, L., Ananthan, S., Zhang, Z., Hutchings, K., Wang, P., Chen, W., and Chen, L.: Field test of wake steering at an offshore wind farm, Wind Energy Science, 2, 229–239, https://doi.org/10.5194/wes-2-229-2017, 2017.

Guo, F., Mann, J., Peña, A., Schlipf, D., and Cheng, P. W.: The space-time structure of turbulence for lidar-assisted wind turbine control, Renewable Energy, 2022.

Guo, F., Schlipf, D., and Cheng, P. W.: Evaluation of lidar-assisted wind turbine control under various turbulence characteristics, Wind Energy Science, 8, 149–171, https://doi.org/10.5194/wes-8-149-2023, 2023.

Kaimal, J. C., Wyngaard, J., Izumi, Y., and Coté, O.: Spectral characteristics of surface-layer turbulence, Quarterly Journal of the Royal Meteorological Society, 98, 563–589, 1972.

Liew, J., Urbán, A. M., and Andersen, S. J.: Analytical model for the power–yaw sensitivity of wind turbines operating in full wake, Wind Energy Science, 5, 427–437, 2020.

Lundquist, J. K., Churchfield, M. J., Lee, S., and Clifton, A.: Quantifying error of lidar and sodar Doppler beam swinging measurements of wind turbine wakes using computational fluid dynamics, Atmospheric Measurement Techniques, 8, 907–920, https://doi.org/10.5194/amt-8-907-2015, 2015.

Mann, J.: The spatial structure of neutral atmospheric surface-layer turbulence, Journal of fluid mechanics, 273, 141–168, 1994.

Mann, J.: Wind field simulation, Probabilistic engineering mechanics, 13, 269–282, 1998.

Mikkelsen, T., Angelou, N., Hansen, K., Sjöholm, M., Harris, M., Slinger, C., Hadley, P., Scullion, R., Ellis, G., and Vives, G.: A spinner-integrated wind lidar for enhanced wind turbine control, Wind Energy, 16, 625–643, https://doi.org/10.1002/we.1564, 2013.

Mikkelsen, T., Astrup, P., and van Dooren, M.: The Lidar Cyclops Syndrome Bypassed: 3D Wind Field Measurements from a Turbine mounted Lidar in combination with a fast CFD solver, http://isars2016.org/, 18th International Symposium for the Advancement of Boundary-Layer Remote Sensing, ISARS 2016 ; Conference date: 06-06-2016 Through 09-06-2016, 2016.

Piomelli, U.: Large-eddy simulation: achievements and challenges, Progress in aerospace sciences, 35, 335–362, 1999.

https://doi.org/10.5194/wes-2023-162
Preprint. Discussion started: 11 January 2024

Raach, S., Schlipf, D., Haizmann, F., and Cheng, P. W.: Three Dimensional Dynamic Model Based Wind Field Reconstruction from Lidar Data, Journal of Physics: Conference Series, 524, https://doi.org/10.1088/1742-6596/524/1/012005, 2014.

Sathe, A. and Mann, J.: Measurement of turbulence spectra using scanning pulsed wind lidars, Journal of Geophysical Research: Atmospheres, 117, 2012.

Sathe, A., Banta, R., Pauscher, L., Vogstad, K., Schlipf, D., and Wylie, S.: Estimating turbulence statistics and parameters from ground-and nacelle-based lidar measurements: IEA Wind expert report, 2015.

Schlipf, D.: Lidar-Assisted Control Concepts for Wind Turbines, Ph.D. thesis, University of Stuttgart, 2016.

Schlipf, D., Kapp, S., Anger, J., Bischoff, O., Hofsäß, M., Rettenmeier, A., and Kühn, M.: Prospects of optimization of energy production by lidar assisted control of wind turbines, 2011.

Schlipf, D., Koch, M., and Raach, S.: Modeling uncertainties of wind field reconstruction using lidar, in: Journal of Physics: Conference Series, vol. 1452, p. 012088, IOP Publishing, 2020.

Simley, E. and Pao, L.: Reducing LIDAR wind speed measurement error with optimal filtering, in: 2013 American Control Conference, pp. 621–627, IEEE, 2013.

Simley, E., Pao, L., Frehlich, R., Jonkman, B., and Kelley, N.: Analysis of wind speed measurements using continuous wave LIDAR for wind turbine control, in: 49th AIAA Aerospace Sciences Meeting including the New Horizons Forum and Aerospace Exposition, p. 263, 2011.

Smith, D. A., Harris, M., Coffey, A. S., Mikkelsen, T., Jørgensen, H. E., Mann, J., and Danielian, R.: Wind lidar evaluation at the Danish wind test site in Høvsøre, Wind Energy, 9, 87–93, https://doi.org/10.1002/we.193, 2006.

Towers, P. and Jones, B. L.: Real-time wind field reconstruction from LiDAR measurements using a dynamic wind model and state estimation, Wind Energy, 19, 133–150, 2016.

Von Karman, T.: Progress in the statistical theory of turbulence, Proceedings of the National Academy of Sciences, 34, 530–539, 1948.

Zhang, L. and Yang, Q.: A Method for Yaw Error Alignment of Wind Turbine Based on LiDAR, IEEE Access, 8, 25 052–25 059, https://doi.org/10.1109/ACCESS.2020.2969477, 2020.

Zhang, Z., Bakhoday-Paskyabi, M., Schito, P., Reuder, J., and Zasso, A.: Wind Farm Inflow Wind Simulation based on Mesoscale and Microscale Coupling, in: Journal of Physics: Conference Series, vol. 2265, p. 022044, IOP Publishing, 2022.

Zhao, H., Zhou, L., Zhang, S., and Liang, Y.: XE112-2000 Wind Turbine Yaw Strategy With Adaptive Yaw Speed Using DEL Look-Up Table, IEEE Access, 9, 125 724–125 738, https://doi.org/10.1109/ACCESS.2021.3111188, 2021.